D. Argence, J. Weiss,† and A. Pineau**

Observation and Modelling of Transgranular and Intergranular Multiaxial Low-Cycle Fatigue Damage of Austenitic Stainless Steels

REFERENCE Argence, D., Weiss, J., and Pineau, A., **Observation and modelling of transgranular and intergranular multiaxial low-cycle fatigue damage of austenitic stainless steel,** *Multiaxial and Fatigue Design*, ESIS 21 (Edited by A. Pineau, G. Cailletaud, and T. C. Lindley) 1996, Mechanical Engineering Publications, London, pp. 209–227.

ABSTRACT The aim of the present study is to observe and model the physical damage induced by multiaxial (tension–torsion) low-cycle fatigue of 316 austenitic stainless steel tested both at room temperature and at 600°C. Four heats with slightly different chemical compositions are compared. Various types of experiments were carried out on thin tubular specimens: (i) continuous pure transgranular fatigue tests; (ii) sequential tests at 25°C and 600°C with both types of sequences, i.e. tension → torsion tests and the opposite; (iii) multiaxial intergranular creep-fatigue tests at 600°C with a superimposed hold time at maximum strain; (iv) sequential fatigue/creep-fatigue tests. A change in the orientation of crack initiation sites was observed both in tension and in torsion between room temperature and 600°C. At elevated temperature, state I crack initiation which occurs under shear mode is bypassed by the effect of oxidation. Moreover, sequential tests showed a large detrimental effect when both crack initiation and crack growth are coplanar. This explains why at room temperature the most damaging sequence is that of torsion → tension, whereas at elevated temperature the opposite is observed. It is also shown that minor compositional modifications may have a signficant influence on the endurance of the materials when they are tested under creep-fatigue conditions. This sensitivity to hold time effect is related to carbide precipitation and to creep intergranular cavitation damage. A stochastic model based on two-dimensional Monte-Carlo simulation is proposed. This model, which accounts very well for the situations in which both crack initiation and crack growth are coplanar, includes damage equations based on quantitative metallographical observations. Damage is modelled as the continuous nucleation of a population of growing cracks which eventually coalesce to lead to final fracture. This model is able to reproduce the fatigue lives measured under multiaxial continuous and sequential tests, and to predict the scatter and the size effect observed in fatigue testing.

Introduction

Most structural components are subjected in service to complex low-cycle fatigue (LCF) loading conditions, in particular in regions of stress concentrations, which

*Centre des Matériaux, Ecole des Mines, BP 87, 91003 Evry Cedex, URA CNRS 866, France.
† Laboratoire de Glaciologie et Geóphysique de l'Environment, BP 96, 38402 St Martin d'Heres Cedex, 4PR CNRS 5151, France.

lead eventually to fatigue crack initiation and crack propagation. This occurs, in particular, in power generating components which are often fabricated from austenitic stainless steels, when they are submitted to superimposed mechanical and thermal stresses. These components are subjected to a combination of cyclic and creep loading which is usually referred to as creep-fatigue (CF).

For a long time, most of the studies dealing with fatigue and CF damage of austenitic stainless steels at elevated temperature have been limited to uniaxial (mainly tensile) conditions. These studies have shown that the application of a tensile hold time at maximum strain of a fatigue cycle may produce a significant reduction of the LCF endurance of type 304 and 316 stainless steels (**1–7**). This reduction in fatigue life is qualitatively explained by the formation of creep intergranular cavitation damage which interacts with transgranular fatigue damage. A number of authors (**4–7**) have developed models which take into account quantitatively this interaction. The validation of these models derived from uniaxial tests to multiaxial loadings is clearly a major area of concern for both the engineers and the materials scientists. This necessitates not only further multiaxial tests but also detailed observations concerning, in particular, the directional aspect of both the fatigue and the creep damage.

Brown and Miller (**8–9**) were among the first investigators to emphasize the importance of the directional aspect of fatigue damage under multiaxial loading. At room temperature, in the absence of any pronounced environmental effects, fatigue cracks initiate on shear planes from persistent slip bands, whereas they propagate usually under tensile mode I, except for loading conditions approaching those of pure shear, that is at large values of the ratio $\lambda' = \Delta\gamma/\Delta\varepsilon$. between the shear strain range, $\Delta\gamma$, and the tensile strain range, $\Delta\varepsilon$, and for large values of $\Delta\gamma$.

For large shear strain ranges, crack propagation occurs under shear modes II and III (**10**). This behaviour is one of the reasons which is usually advanced to explain the fact that, at room temperature, the fatigue life of austenitic stainless steel tested under torsional loading is much larger than that measured under push-pull conditions. At elevated temperature, the situation may be quite different due either to strong environmental effects and/or the presence of additional intergranular damage. Unfortunately there is still only a limited number of studies devoted to high-temperature multiaxial LCF. However it is worth mentioning the work performed on 304 stainless steel, (**11**), which showed that, contrary to the situation observed at room temperature, crack initiation occurs under mode I. More recently two of the present authors showed also that, in one heat of 316 stainless steel (SQ steel), stage I crack initiation was bypassed at elevated temperature when the material was tested under air environment but not under vacuum (**12, 13**). These modifications in the orientation of crack initiation sites was attributed to the presence of a brittle oxide film formed at the surface of the specimens. In the above study it was also shown that one of the best methods to study the directional aspect of fatigue damage is to carry out sequential LCF tests. For instance, push-pull

loading followed, during the second part of the sequence, by torsional loading (or the opposite) can lead to cumulative damage much different from that expected by considering each loading type separately (**14**). This is one of the main reasons why in the present study sequential pure fatigue (PF) or CF loadings were also largely used to investigate the effects of the orientation of microcracks on the fatigue life.

It is well known that slight compositional modifications have no significant effect on the LCF life of the materials, in particular of the large family of austenitic stainless steels, when they are tested under pure continuous fatigue, especially at room temperature. On the other hand, the situation may be quite different at elevated temperature, in particular under CF conditions (**4**). Intergranular cavitation can then be facilitated by carbide precipitation and/or impurity segregation along the grain boundaries (**15–17**). This is one of the reasons why in the present study four heats of 316 L type stainless steel with slight differences in chemical composition were investigated.

The aims of the present work are:

(i) To study the influence of multiaxial (tension–torsion) loading on the fatigue and the creep-fatigue life of four heats of 316 L austenitic stainless steels with minor differences in chemical composition;
(ii) To investigate the effect of sequential multiaxial loadings on the fatigue damage mechanisms in relation with the orientation of the microcracks generated during the first part of the sequence. This part of the work has already been partly reported elsewhere (**12, 13**) but more details are given in the present study;
(iii) To identify the nature of the oxides formed at the free surface of the specimens and to determine the growth kinetics of these oxide films.

The results of these tests and of these observations are used to introduce briefly a damage model which was developed previously, based on the interaction between a population of microcracks.

2 Experimental Procedures

2.1 *Materials*

Four heats of 316L austenitic stainless steel were examined. Their composition and their tensile mechanical properties measured at 600°C are reported in Tables 1 and 2, respectively. The details concerning SP, SQ, and 316 MN steels are given elsewhere (**13**). SR steel was annealed at 1100°C, which resulted in a grain size of about 30 μm. This material contained also some ferrite ($\sim$2.7 percent in the centre of the plate), compared to 0.9 percent and 0.4 percent in SP and SQ steels, respectively. This resulted in a larger anisotropy effect, as shown later.

Table 1 Chemical composition (weight percent)

Steels	C	S	P	Si	Mn	Ni	Cr	Mo	N	B	Co	Cu
SP	0.021	0.0080	0.033	0.41	1.74	12.27	17.18	2.40	0.080	0.0032	0.210	0.150
SQ	0.028	0.0010	0.028	0.30	1.88	12.46	17.31	2.44	0.077	0.0012	0.135	0.175
SR	0024	00030	0.018	0.33	1.70	12.10	17.40	2.33	0.072	0.0010	0.200	0.130
316 MN	0.011	0.057	0.028	0.47	0.85	11.07	16.64	2.14	0.068	—	—	—

Table 2 Tensile properties at 600°C

Steels	E (10^3 MPa)	μ (10^3 MPa)	0.2% yield stress (MPa)	UTS (MPa)	Elongation (%)	Reduction of area (%)
SP	144	55	154	407	41	67
SQ	144	55	144	404	41	67
SR	132	58	131	—	—	65
316 MN	146	56	—	390	—	62

2.2 *Mechanical tests*

Thin tubular specimens with an outer diameter of 19.5 mm and a wall thickness of 1.5 mm were tested with a servo-hydraulic tension–torsion machine under strain control conditions. Four types of experiments were performed:

(1) Multiaxial continuous LCF tests, at 25°C and 600°C with a sinusoidal fully reversed wave form at a frequency of 0.05 Hz. These tests included both push-pull and torsion equipments.
(2) Sequential LCF tests at 25°C and 600°C. Both types of sequences were investigated: tension → torsion tests and torsion → tension tests.
(3) Multiaxial continuous CF tests at 600°C by applying a hold time of 30 mm or 60 mm at maximum tensile strain. Both push-pull and torsion tests were carried out.
(4) Fatigue/creep-fatigue sequential tests in which a first sequence of fatigue (or creep-fatigue) loading is followed by a second sequence of creep-fatigue (or fatigue), or the opposite.

Most of the tests were carried out at a von Misès equivalent total strain amplitude of $\Delta\varepsilon_{teq}/2 = \pm 0.8$ percent, except otherwise stated. In particular SP material was tested in continuous tension and torsion fatigue over a broader range of deformation.

3 Results and Discussion

3.1 *Mechanical behaviour*

The results of continuous pure fatigue tests carried out on the four materials both at 25°C and at 600°C are shown in Fig. 1(a) and (b), respectively.

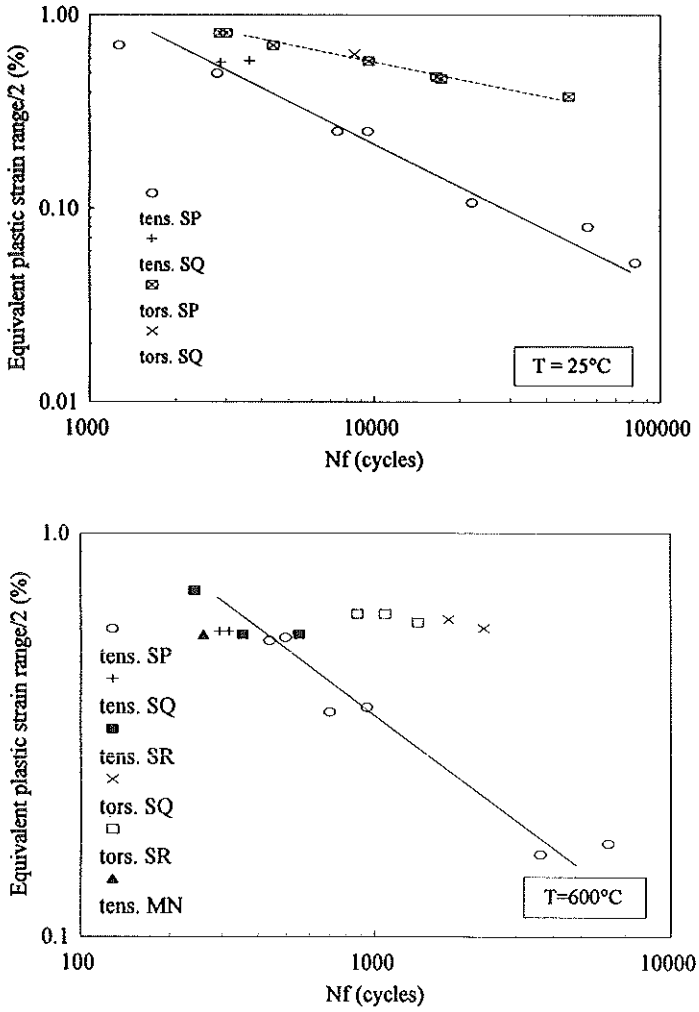

Fig 1 Continuous fatigue lives of SP, SQ, SR and MN steels tested under push-pull and torsion loadings at (a) room temperature; (b) 600°C.

At room temperature, it is noticed that the fatigue lives of SP and SQ materials are similar in spite of their slight difference in chemical composition. This behaviour is observed both in tension and in torsion. At 600°C, which is the temperature used to compare all the materials, the fatigue lives under push-pull conditions are similar. However in all cases it is observed that, whatever the temperature, the fatigue life under fully reversed torsion is much larger than under push-pull conditions. These results are in agreement with those obtained

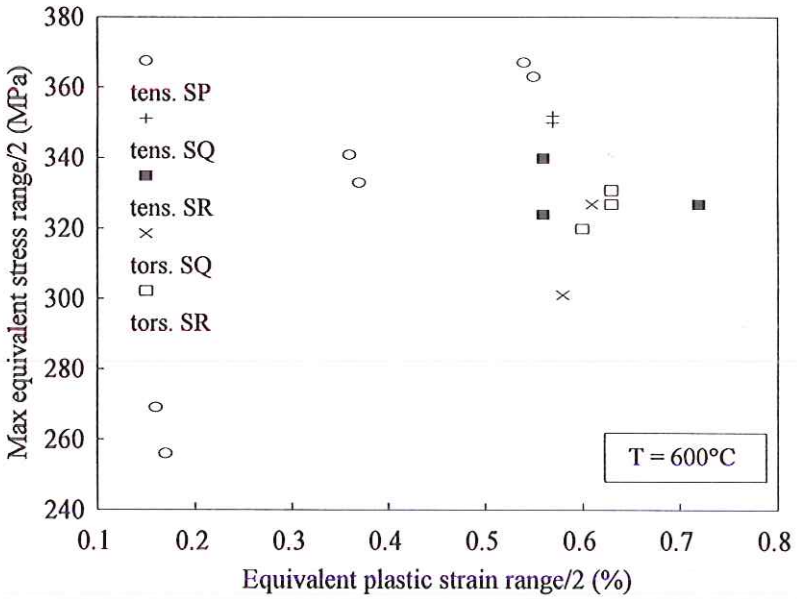

Fig 2 Cyclic stress–strain curves determined in continuous fatigue of SP, SQ, SR and MN steels tested under push-pull and torsion loadings at 600°C.

previously on another heat of 316 L (**18**). The relatively smaller fatigue endurance of SR material tested in torsion is related to the presence of the segregated zone, rich in ferrite, located in the centre of the plate, as indicated earlier. A close examination of the fracture surface of the torsion specimens showed that the shear cracks were aligned with the specimen axis (and not perpendicular as observed in the other materials), and preferentially located in the segregated plane located at midthickness of the plate.

The cyclic stress–strain curves corresponding to the continuous pure fatigue tests carried out at 600°C are shown in Fig. 2. These curves were drawn using the definition of the von Misès equivalent stress (or strain). It is observed that SP, SQ and MN steels are slightly stronger than SR material under push-pull conditions. Moreover, in all cases, except SR material, it is noticed that it is impossible to draw a unique cyclic stress–strain curve using the von Misès equivalent amplitudes. A similar behaviour was noticed at room temperature (**19**).

The relative reductions in fatigue life measured in CF tests carried out at 600°C and at the same total strain amplitude ($\Delta\varepsilon_{teq}/2 = \pm 0.80$ percent) are reported in Fig. 3. It is observed that these reductions are much smaller in SP and MN steels, compared to SQ and SR materials. In the latter materials the fatigue life measured either in tension or in torsion is reduced by a factor of two when a hold time of 30 mn is applied at maximum strain.

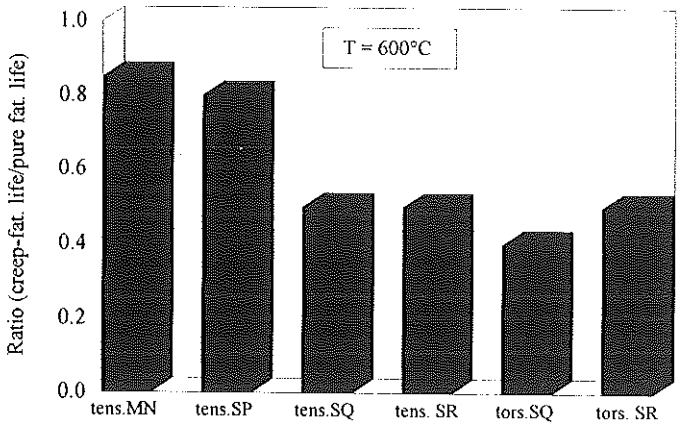

Fig 3 Reduction of fatigue lives of SP, SQ, SR and MN steels between pure fatigue and creep-fatigue tests at 600°C and $\Delta\varepsilon_{teq}/2 = \pm 0.80$ percent – push-pull and torsion loadings.

The results of sequentials tests are shown in Fig. 4. Pure fatigue sequential tests carried out on SQ steel tested both at 25°C and 600°C at $\Delta\varepsilon_{teq}/2 = \pm 0.80$ percent are given in Fig. 4a and b, respectively. In Fig. 4, the damage $D_1 = N_1/Nf_1$ represents the fraction of the fatigue life applied during the first part of the sequential loading, while $D_2 = N_2/Nf_2$ is the relative remaining fatigue life measured during the second part. Large deviations from the Miner linear cumulative damage rule ($D_1 + D_2 = 1$) are observed. Moreover an antisymmetric behaviour is observed since, at a given temperature, an opposite effect is observed between push-pull → torsion sequence and the opposite sequence. At 25°C the remaining push-pull fatigue life is significantly reduced by prior torsion loading, whereas initial push-pull loading has much less effect on the remaining torsional life. This behaviour is similar to the situation reported by other authors (**14**, **20**, **21**). At 600°C the opposite effect is observed since, this time, the most damaging loading is the push-pull → torsion sequence. A small value of the initial damage, D_1, applied under tensile conditions produces a significant reduction of the remaining torsional life.

The results of sequential CF tests obtained on SQ and SR steels are given in Fig. 4c. These tests were carried out in order to investigate the interactions between intergranular and transgranular damage. It is observed that prior intergranular damage introduced by tensile loading produces only slight deviations from the Miner linear rule when the remaining life is measured under push-pull conditions.

The most interesting results are those obtained with a change in the loading mode between both parts of the sequence. It is confirmed that a prior push-pull damage, which produces in this case, both transgranular and intergranular damage, generates a large reduction in the remaining continuous torsional life.

(a)

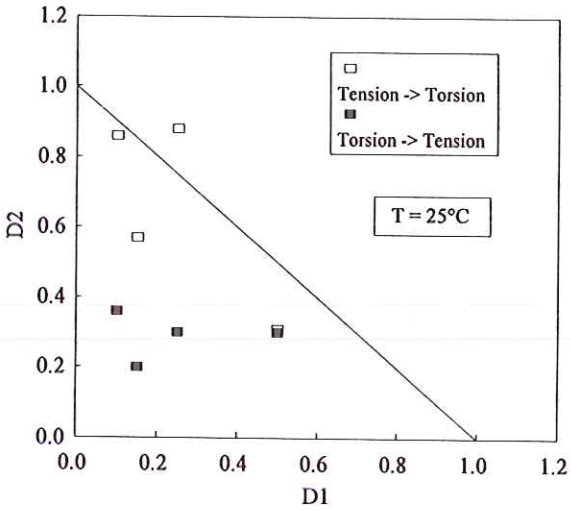

(b)

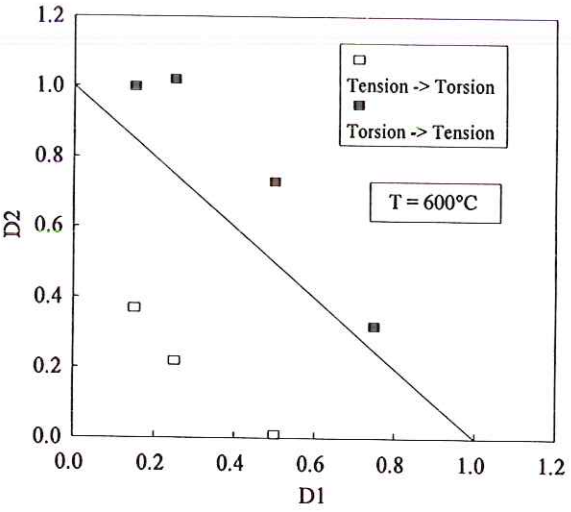

Fig 4a,b Cumulative fatigue and CF damage of sequential loadings on SQ and SR steels at (a) room temperature; (b)(c) 600°C.
(a)(b) push-pull (PF) → torsion (PF) and torsion (PF) → push-pull (PF) sequences.
(c) push-pull (CF) → push-pull (PF), push-pull (CF) → torsion (PF) and push-pull (PF) → torsion (CF) sequences.

This situation is similar to that observed previously (Fig. 4b). On the other hand this damaging effect is not observed when the torsional loading applied during the second part of the sequence includes a hold time. In that case the cumulative damage may even be larger than one, which may appear to be somewhat surprising.

(c)

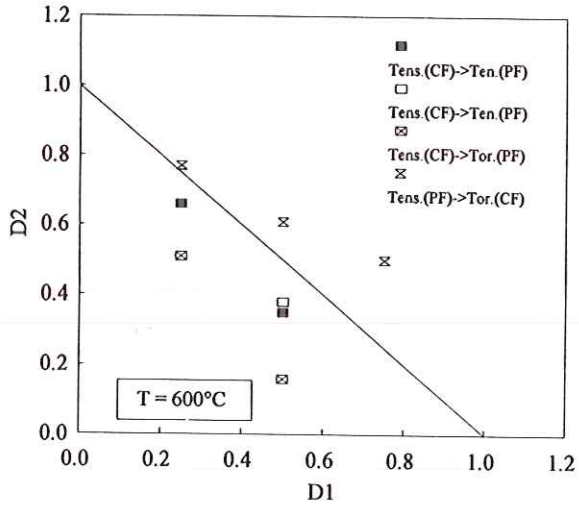

Fig 4c Cumulative fatigue and CF damage of sequential loadings on SQ and SR steels at (a) room temperature; (b)(c) 600°C.
(a)(b) push-pull (PF) → torsion (PF) and torsion (PF) → push-pull (PF) sequences.
(c) push-pull (CF) → push-pull (PF), push-pull (CF) → torsion (PF) and push-pull (PF) → torsion (CF) sequences.

3.2 *Metallurgical observations and damage measurements*

Pure fatigue

Pure fatigue damage is associated with the formation of a population of transgranular microcracks nucleated on the free surface of the specimens which propagate and coalesce as a main crack. Both the free surface and longitudinal sections of the specimens were observed to measure the orientation as well as the density of these microcracks. The crack density measurements, in addition to striation spacing measurements made on the fracture surfaces, were used to assess the fatigue crack growth rate (FCGR). Full details are given elsewhere **(6, 7, 12, 13)**. It was shown that at 25°C microcracks nucleate on maximum shear planes which correspond to stage I crack initiation. On the other hand, at 600°C, microcracks nucleate in opening mode. This was observed both under push-pull and torsional conditions, as indicated schematically in Fig. 5.

The surface density of microcracks with a length of the order of the grain size (~ 25 μm), χ, was shown to increase linearly with the number of applied cycles, N. For push-pull conditions at 600°C

$$\underset{(\mu m^{-2})}{\chi} = \underset{}{\chi_0} \times \underset{(\%)}{(\Delta\varepsilon_p/2)^4} \times \underset{(\text{cycles})}{N} \qquad (1)$$

where $\chi_0 = 8 \times 10^{-7}$.

For torsional loading at 25°C, it was found that the surface density was not dependent on the plastic shear strain amplitude, $\Delta\gamma_p/2$, at least in the relatively

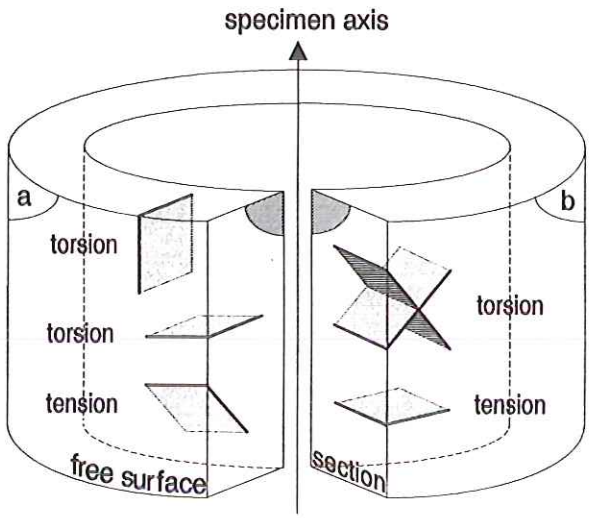

Fig 5 Orientation of continuous fatigue microcracks determined on specimen free surface and longitudinal sections for push-pull and torsion loadings at (a) room temperature; (b) 600°C ($\Delta\varepsilon_{teq}/2 = 0.80$ percent).

small range of $\Delta\gamma_p/2$ values explored in this study. The corresponding surface density was expressed as

$$\chi = \chi_0 N \tag{2}$$

where $\chi_0 = 8 \times 10^{-9}$

In all cases, it was observed that the macrocracks formed by the coalescence of microcracks propagate under mode I for push-pull conditions, while they grow along maximum shear planes under torsional loading. It was observed that the crack front adopts a semi-elliptical shape with an aspect ratio, q = small axis length/large axis length, equal to ~ 1 for tensile loading and to ~ 0.5 for torsional loading. The crack growth laws were expressed for push-pull loading as

$$\underset{(\mu m/cycle)}{da/dN} = A \times \underset{(\%)}{(\Delta\varepsilon_p/2)^{\alpha}} \times \underset{(\mu m)}{a^{\beta}} \tag{3}$$

where $\alpha = 1.5$ and $\beta = 1.45$, while $A = 6.8 \times 10^{-4}$ at 25°C and $A = 3.1 \times 10^{-3}$ at 600°C. For torsional loading

$$\underset{(\mu m/cycle)}{da/dN} = C \times \underset{(\%)}{(\Delta\gamma_p/2)^{\alpha'}} \times \underset{(\mu m)}{a^{\beta'}} \tag{4}$$

where $\alpha' = 3.7$ and $\beta' = 2.6$, while $C = 7.9 \times 10^{-7}$ at 600°C

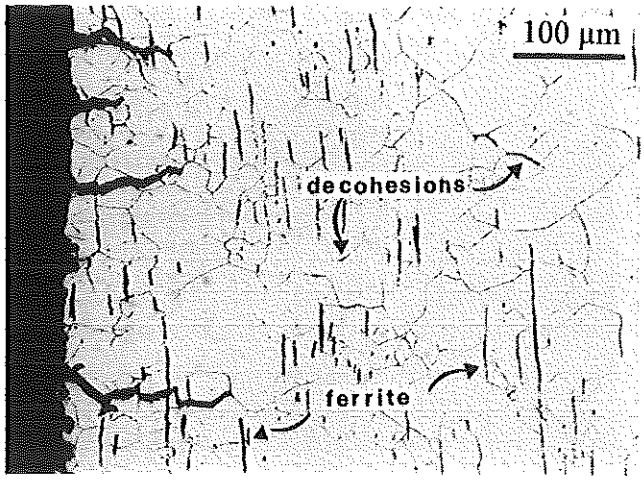

(a)

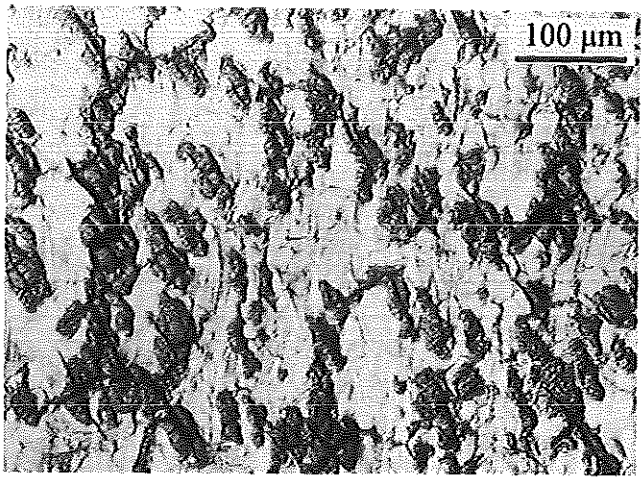

(b)

Fig 6 SR specimen tested under torsion (CF) loading at 650°C with $\Delta\varepsilon_{1eq}/2 = \pm 0.80$ percent and $t_m = 30$ mn. (a) Optical observation of a longitudinal section showing intergranular and transgranular surface microcracks and intergranular bulk decohesions. (b) SEM observation of the free surface Mode I microcracks coalesce in the direction of specimen axis and are associated with heavy oxidation.

Creep-fatigue experiments

The application of a hold time at maximum strain tends to produce intergranular damage which was observed both at the free surface and in the bulk of the specimens. This is illustrated in Fig. 6a which corresponds to a specimen of SR steel tested at a higher temperature of 650°C. Quantitative measurements of

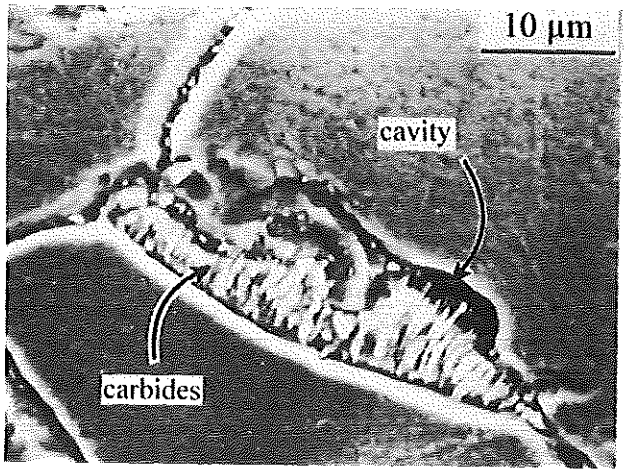

(a)

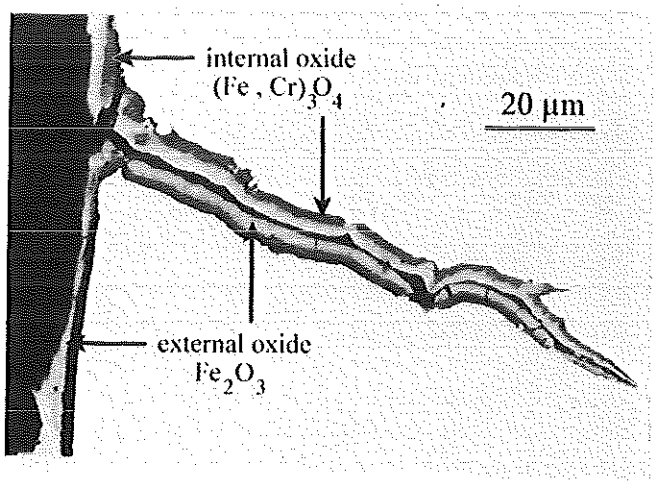

(b)

Fig 7 SR specimen tested under push-pull (CF) loading at 600°C with $\Delta\varepsilon_{teq}/2 = \pm 0.80$ percent and $t_m = 60$ mn. (a) Grain boundaries SEM observation of $M_{23}C_6$ carbide precipitation with cellular reaction and a docohesion. (b) Optical observation of a longitudinal section with internal $(Fe, Cr)_3O_4$ and Fe_2O_3 oxides layers.

intergranular damage were made on SP, SQ and MN steels. These results are reported elsewhere (13). Here it is enough to mention that SP and MN materials contained much less intergranular damage, compared to SQ steel. In particular 316 MN steel contained no intergranular damage when tested at 600°C with a hold time of 30 mn. These differences between the behaviour in creep-fatigue of low carbon (316 L) and extra low carbon (316 MN) steels shown in Fig. 3

are in good agreement with the results obtained by Nakazawa *et al.* (**22**). Detailed examinations showed that the intergranular bulk damage, that is the decohesions along the grain boundaries, when present, were preferentially oriented perpendicular to the maximum principal stress σ_1, positive during the hold time (**13**).

The propagation of the macrocracks was partly intergranular, especially in the materials (SQ and SR steels) which gave rise to heavy grain boundary cavitation. Under these conditions, in particular in SQ steel, and under torsional loading, the crack propagation plane tended to shift from the maximum shear strain plane to the plane corresponding to the maximum principal, σ_1, positive during the hold time. In SR steel which exhibited a stronger anisotropy effect, as indicated earlier, the propagation plane remained aligned with the specimen axis, as illustrated in Fig. 6b. In this figure, it is observed that crack propagation occurs by the coalescence of mode I microcracks in the direction of the specimen axis. It is also noted that heavy oxidation takes place preferentially in the vicinity of the coalesced microcracks.

Another difference between the four investigated materials was related to $M_{23}C_6$ carbide precipitation along the grain boundaries. These carbides appeared either as isolated or as massive precipitates. An example of massive precipitation in the form of parallel platelets, crystallographically oriented with one of the grains (**23**) is shown in Fig. 7a. This precipitation was not observed in SP and 316 MN steels tested under the same conditions.

Intergranular carbide precipitation in austenitic stainless steels has largely been investigated in the literature (**15**). These materials may give rise to $M_{23}C_6$ carbide precipitation, depending in particular on their carbon content, during thermal exposure but this precipitation is accelerated by cyclic deformation (**13**). The extra low carbon content in 316 MN steel and, to some extent, in SP steel shifts the carbide precipitation to longer times. A higher boron content in SP steel may also contribute to the improved thermal stability of this material, since it is well known that this element has a strong influence on creep ductility of austenitic stainless steels (**24**) by reducing intergranular precipitation which, in turn, produces a reduction in intergranular cavitation (**25**). These differences in thermal stability between the various materials might partly explain their different behaviours observed in CF experiments (Fig. 3).

Sequential tests

The observations showing that prior torsional fatigue at 25°C produces a large detrimental effect (Fig. 4a) can be explained by the fact that shear microcracks nucleated by torsion can easily propagate in mode I during tensile loading, when they are located perpendicular to the specimen axis. Similarly, at 600°C, the microcracks initiated in opening mode during either PF or CF push-pull conditions are located along preferential shear planes during the second torsional part of the sequence. These observations indicate that a cumulative damage D lower than one is obtained in sequential fatigue when the initiation planes of the first phase and the propagation planes of the second one are coplanar. On

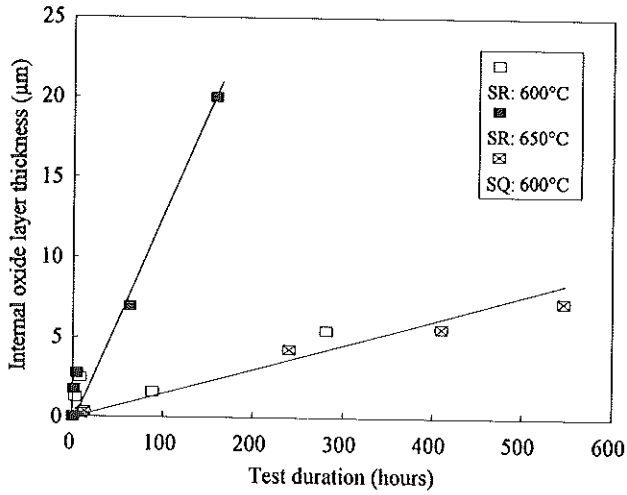

Fig 8 Internal oxide layer thickness on SQ and SR steels tested at 600°C and 650°C.

the other hand a cumulative damage larger than one is observed when these planes do not coincide, that is when the microcracks initiated during the first part of the sequence have to bifurcate to propagate during the second part, as shown schematically in Fig. 5. The difference in the orientation of crack initiation sites between 25°C and 600°C explains the differences observed in the cumulative diagrams of sequential pure fatigue tests (Fig. 4a and b).

A close examination of the specimens submitted to the pure tensile fatigue → torsional creep-fatigue sequence (Fig. 4c) provided an explanation for the observed behaviour which may seem to be anomalous. The microcracks initiated during prior tensile loading were found to be healed by the presence of a thick oxide film. Under these conditions a new family of initiation sites, typical of torsional loading, that is aligned along the maximum principal stress, was formed. In these tests crack healing by oxide formation was facilitated in the long time period imposed by this mode of loading. This explains qualitatively the fact that under these conditions a cumulative damage larger than one was found.

3.3 *Oxidation behaviour*

In the absence of deformation a very thin layer of Cr_2O_3 grows on the free surface of austenitic stainless steels. This oxide protects the material against further oxidation. Preferential oxidation takes place in the vicinity of microcracks (Fig. 6b). Another example of the oxide layers formed at the free surface of fatigue specimens of SQ steel is shown in Fig. 7b where it is also observed that preferential oxidation takes place along the fatigue cracks. Two types of oxides,

different to Cr_2O_3, were identified in the four investigated materials when they were cyclically deformed:

(a) an external layer of FeO_3, oxide (Hematite);
(b) an internal layer of $(Fe, Cr)_3O_4$ oxide which was shown to have the same crystallographic nature as that of chromite, $FeCr_2O_4$.

The thickness of the external layer was very irregular. The mean thickness of the internal layer versus testing duration is shown in Fig. 8. The results were obtained on SQ steel at 600°C and on SR steel tested both at 600°C and 650°C. In both cases, except for pure fatigue tests which lasted a short time period, it is observed that the kinetics of oxidation are different from the classical parabolic law since the thickness of the oxide layer increases linearly with time. The role of cyclic plasticity was also clearly illustrated since preferential growth of $(Fe, Cr)_3O_4$ oxide along intense slip bands was observed. In Fig. 8 it is noted that the increase in test temperature from 600°C to 650°C produces an acceleration of the oxidation kinetics by almost one order of magnitude.

It was thus observed that the interaction between oxidation and cyclic deformation produces three mains effects

(a) a modification in the initiation modes when the test temperature is increased from 25°C to 600°C;
(b) a strong reduction of the fatigue lives at high temperature when the materials are tested under air environment;
(c) in a number of circumstances, such as the pure tensile fatigue → torsional creep-fatigue sequence, a beneficial effect is associated with microcrack healing effect.

3.4 *Modelling*

In the present study it was clearly shown that a classical linear cumulative damage rule is unable to account for the results of sequential fatigue, in particular those of pure transgranular fatigue. The present authors have therefore developed an approach based on the physical description of fatigue damage, that is the nucleation, the growth, and the final coalescence of microcracks to model these results. This model applies only to situations in which both crack initiation and crack propagation are coplanar, i.e. those for which the cumulative damage is smaller than one (Fig. 4). Moreover, at the time being, the model applies only to pure transgranular fatigue. The extension of the approach to creep-fatigue conditions is under development. In the present paper only a brief account of the model is given. More details can be found elsewhere (**13, 26, 27**).

The main interest of the approach lies in the fact that it is directly based on the relations obtained from metallographical observations, describing both the nucleation and the growth of a population of microcracks, equations (1–4). The only stage which is poorly understood is that of crack coalescence. For this purpose, an influence zone, similar to the plastic zone of the Dugdale–

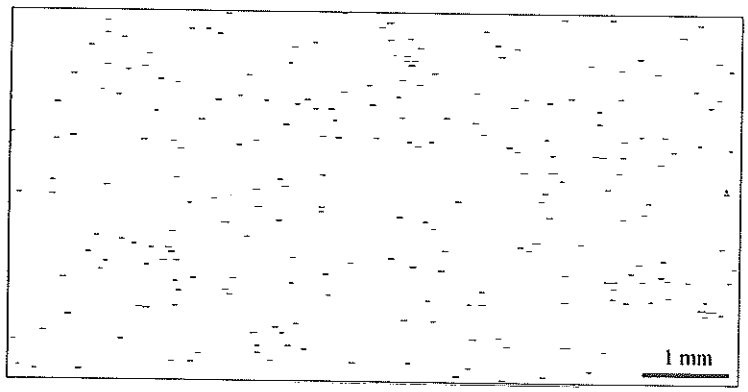

(a)

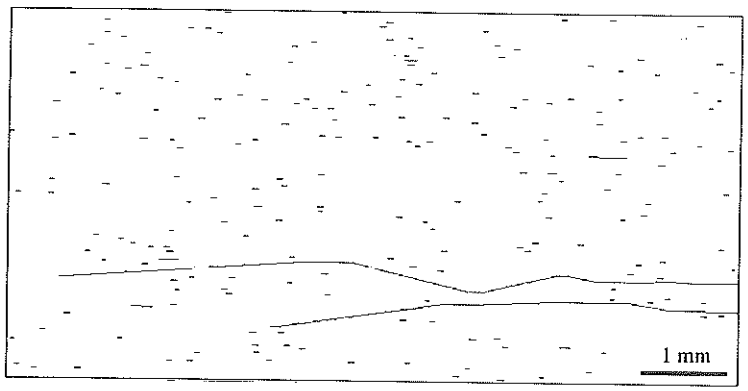

(b)

Fig 9 Monte-Carlo type simulation of a sequential continuous fatigue push-pull → torsion test at 600°C with $\Delta\varepsilon_{teq}/2 = \pm 0.80$ percent. (a) 2 cycles in torsion after 75 cycles in tension-compression. (b) 338 cycles in torsion after 75 cycles in tension–compression.

Barenblatt model (**28**) was introduced, such as crack coalescence is assumed to take place when the plastic zones associated with two neighbouring cracks are overlapping. This produces a strong acceleration of the local FCGR corresponding to the two coalesced cracks. A second interest of the model lies in the fact that is based on a statistical approach. The description of the behaviour of nucleating and growing microcracks is based on a two-dimensional Monte-Carlo type simulation. The surface is represented by a grain matrix with a mean grain size of 50 μm. Initiation sites of microcracks located within these grains are selected by a Poisson process which was shown to simulate satisfactorily

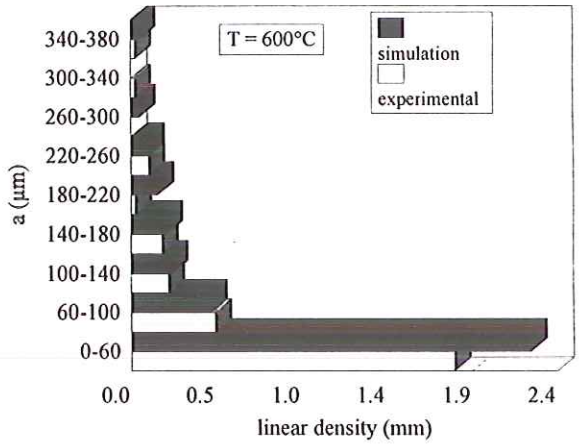

Fig 10 SQ steel tested under push-pull (PF) loading at 600°C with $\Delta\varepsilon_{teq}/2 = \pm 0.80$ percent. Comparison of measured and simulated microcracks distribution.

the experimental situation (**26, 27**). The size of the nucleating microcracks is taken as equal to 50 μm, whereas the density increases linearly with the number of cycles, according to equations (1, 2). The length of each microcrack increases according to the growth laws given by equations (3, 4). The coalescence criterion introduced earlier is tested continuously.

An example obtained with this simulation applied to sequential tensile → torsion test is shown in Fig. 9. This figure illustrates the dramatic effect of torsional loading on a population of microcracks nucleated from a prior push-pull loading applied at 600°C. This effect is similar to the situation observed experimentally (Fig. 4).

The main results obtained from this simulation can be summarized as follows.

(1) The model is able to simulate correctly the continuous fatigue life of specimens tested under conditions for which no crack deviation between initiation and growth takes place, such as torsion at 25°C and tension at 600°C. This simulation suggested that crack coalescence occurs more easily under shear mode than under tension.
(2) The model also satisfactorily represents the detrimental effect ($D \ll 1$) of fatigue sequences in which both crack initiation and crack growth are coplanar, that is the torsion → tension sequence at 25°C and the opposite at elevated temperature.
(3) The distributions of crack density calculated from the simulation and those measured experimentally are found to be in good agreement. An example corresponding to a push-pull test at 600°C on SQ material is shown in Fig. 10.
(4) The statistical model is also able to reproduce the statistical scatter observed in fatigue tests and to account for size effects. For continuous fatigue this size effect may be represented by a Weibull law.

4 Conclusions

The fatigue life behaviour measured at 600°C under continuous fatigue does not strongly depend on slight compositional modifications. On the other hand the creep-fatigue life may largely be affected even by small changes in chemical composition, such as the carbon and the boron content. This relative sensitivity to hold time effect is partly related to detrimental intergranular carbide precipitation.

At 600°C, state I crack initiation is bypassed by stress-assisted oxidation.

Nonlinear cumulative damage is observed for sequential multiaxial fatigue. The most damaging effects are observed when crack initiation and crack propagation are coplanar, that is for the torsion → push-pull sequence at room temperature and for the opposite at elevated temperature.

At elevated temperature, oxide formation at the free surface of specimens is considerably altered by cyclic deformation. Both the nature of the oxides and the kinetics of oxide growth are strongly modified.

A two-dimensional stochastic model based on a Monte-Carlo type simulation is shown to reproduce with good accuracy the results of fatigue tests in which no bifurcation takes place between crack initiation and crack growth. This simulation based on quantitative metallographical observations accounts very well for the results of not only continuous fatigue tests but also sequential tests in which crack initiation and crack growth are coplanar.

Acknowledgements

The authors wish to thank the Direction de la Sûreté des Installations Nucléaires (DSIN) for financial support of the project.

References

(1) BRINKMAN, C. R., KORTH, G. E. and HOBBINS, R. R. (1972) Estimates of creep-fatigue interaction in irradiated and unirradiated austenitic stainless steels, *Nuclear Technology*, **16**, 297–307.

(2) WAREING, J. (1975) Fatigue crack growth in a Type 316 stainless steel and a 20% Cr/25% Ni/Nb stainless steel at elevated temperature, *Metallurgical Transactions*, **6A**, 1367–1377.

(3) WOOD, D. S., WYNN, J., BALDWIN, A. B. and O'RIORDAN, P. (1980) Some creep-fatigue properties of Type 316 steel at 625°C, *Fatigue of Engineering Materials and Structures*, **3**, 39–57.

(4) WAREING, J. (1981) Creep-fatigue behaviour of four casts of Type 316 stainless steel, (1981) *Fatigue of Engineering Materials and Structures*, **4**, 131–145.

(5) HALES, R., A quantitative metallographical assessment of structural degradation of Type 316 stainless steel during creep-fatigue, (1980) *Fatigue of Engineering Materials and Structures*, **3**, 339–356.

(6) LEVAILLANT, C. and PINEAU, A. (1980) Assessment of high-temperature low-cycle fatigue of austenitic stainless steels by using intergranular damage as correlating parameter, *Low-Cycle Fatigue and Life Prediction, ASTM STP 770*, (C. Amzallag, B. N. Leis and P. Rabbe eds,) American Society for Testing and Materials, 169–193.

(7) LEVAILLANT, C., GRATTIER, J., MOTTOT, M. and PINEAU, A. (1988) Creep and creep-fatigue intergranular damage in austenitic stainless steels: discussion of the creep dominated regime, *Low-Cycle Fatigue, ASTM STP 942*, (H. D. Solomon, G. R. Halford, L. R. Kaisant and B. N. Leis eds,) American Society for Testing and Materials, Philadelphia, 414–437.

(8) BROWN, M. W. and MILLER, K. J. (1973) A theory for fatigue failure under multiaxial stress-strain conditions, *Proc. Inst. Mech. Eng.*, **187**, 745–755.

(9) BROWN, M. J. and MILLER, K. J. (1979) Initiation and growth of cracks in biaxial fatigue, *Fatigue of Engineering Materials and Structures*, **1**, 231–246.
(10) DOQUET, V. and PINEAU, A. (1991) Multiaxial low-cycle fatigue behaviour of a mild steel, *Fatigue under Biaxial and Multiaxial Loading*, **ESIS 10**, (K. Kussmaul, D. McDiarmid and D. Socie eds,) Mechanical Engineering Publications, London, 81–101.
(11) SAKANE, M. OHNAMI, M. and SAWADA, M. (1987) Fractures modes and low-cycle biaxial fatigue life at elevated temperature, *Journal of Engineering Materials and Technology*, **109**, 236–243.
(12) WEISS, J. and PINEAU, A. (1993) Continuous and sequential multiaxial low-cycle fatigue damage in 316 stainless steel, *Advances in Multiaxial Fatigue*, **ASTM STP 1191**, (D. L. McDowell and R. Ellis eds,) American Society for Testing and Materials, Philadelphia, 183–203.
(13) WEISS, J. and PINEAU, A. (1993) Fatigue and creep-fatigue damage of austenitic stainless steels under multiaxial loading, *Metallurgical Transactions*, **24A**, 2247–2261.
(14) MILLER, K. J. Metal fatigue - past, current and future, (1991) *Proc. Inst. Mech. Eng.*, **205**, 1–14.
(15) WEISS, B. and STICKLER, R. (1972) Phase instabilities during high temperature of 316 austenitic stainless steel, *Metallurgical Transactions*, **3**, 851–866.
(16) JAMES, A. W. and SHEPHERD, C. M. (1989) Some effects of heat treatment on grain boundary chemistery and precipitation in Type 316 steel, *Materials Science and Technology*, **5**, 333–345.
(17) MISVA, R. D. K. and BALASUBRAMANIAN, T. V. (1990) Stress enhanced grain boundary segregation of impurity elements in a low alloy steel, *Acta Metallurgica et Materialia*, **38**, 1263–1266.
(18) JACQUELIN, B., HOURLIER, F. and PINEAU, A. (1985) Crack initiation under low-cycle multiaxial fatigue, *Multiaxial Fatigue*, **ASTM STP 853**, (K. J. Miller and M. W. Brown eds,) American Society for Testing Materials, Philadelphia, 285–313.
(19) DOQUET, V., CAILLETAUD, G. and PINEAU, A. (1991) Cyclic multiaxial behaviour of an austenitic stainless steel: microstructural observations and micromechanical modelling, *Fatigue under Biaxial and Multiaxial Loading*, **ESIS 10**, (K. Kussmaul, D. McDiarmid and D. Socie eds,) Mechanical Engineering Publications, London, 131–149.
(20) ROBILLARD, M. and CAILLETAUD, G. (1991) Directionally defined damage in multiaxial low-cycle fatigue: experimental evidence and tentative modelling, *Fatigue under Biaxial and Multiaxial Loading*, **ESIS 10**, (K. Kussmaul, D. McDiarmid and D. Socie eds,) Mechanical Engineering Publications, London, 103–130.
(21) HARADA, S. and ENDO, T. (1991) On the validity of miner's rule under linearly combined loading of rotating bending and cyclic torsion fatigue under biaxial and multiaxial loading, *Fatigue under Biaxial and Multiaxial Loading*, **ESIS 10**, (K. Kussmaul, D. McDiarmid and D. Socie eds,) Mechanical Engineering Publications, London, 161–178.
(22) NAKAZAWA, T., FUJITA, N., KAGUCHI, K., KANEKO, H. and UEDA, H. (1992) Study on metallography of low-cycle creep-fatigue fracture of Type 316 stainless steels, *Low-Cycle Fatigue and Elasto-Plastic Behaviour of Materials-3*, (K. T. Rie ed.,) Elsevier Applied Science, Berlin, 88–93.
(23) REZGUI, B., PETREQUIN, P. and MOTTOT, M. (1981) Hold time effects on low-cycle fatigue properties of 316L stainless steel at 600 °C and 650 °C, *International Conference on Fracture – 5*, (D. François ed.,) Pergamon Press, Cannes, France, **5**, 2393–2402.
(24) BOURGEOT, J., HENRY, G., MICHAUT, B. and THOMAS, B. (1977) Amélioration de la tenue au fluage d'aciers inoxydables austénitiques stabilisés, etude du rôle de la précipitation, du bore et du traitement d'hypertrempe, *Mémoires Scientifiques, Revue de Métallurgie*, 491–512.
(25) RAJ, R. (1976) Crack initiation in grain boundary under conditions of steady-state and cyclic creep, *Journal of Engineering Materials and Technology*, **98**, 132–139.
(26) WEISS, J. and PINEAU, A. (1992) Microstructurally-based simulation of multiaxial low-cycle fatigue damage of 316L stainless steel in terms of the behaviour of a crack population, *Low-Cycle Fatigue and Elasto-Plastic Behaviour of Materials –3* (K. T. Rie ed,) Elsevier Applied Science, Berlin, 82–87.
(27) WEISS, J. (1992) Endommagement en viscoplasticité cyclique sous chargement multiaxial à haute temperature d'un acier inoxydable austénitique, *PhD Thesis, Ecole Nationale Superieure des Mines de Paris*.
(28) IRWIN, G. R. and PARIS, P. C. (1971) Fundamental aspects of crack growth and fracture, *Fracture, An Advanced Treatise* (H. Liebowitz ed.,) Vol. 3, Academic Press, New-York, 2–44.